

# 3C 286: a bright, compact, stable, and highly polarized calibrator for millimeter-wavelength observations

Iván Agudo<sup>1,2</sup>, Clemens Thum<sup>3</sup>, Helmut Wiese Meyer<sup>4,5</sup>, Sol N. Molina<sup>1</sup>, Carolina Casadio<sup>1</sup>, José L. Gómez<sup>1</sup>, and Dimitrios Emmanoulopoulos<sup>6</sup>

<sup>1</sup> Instituto de Astrofísica de Andalucía, CSIC, Apartado 3004, 18080, Granada, Spain  
e-mail: iagudo@iaa.es

<sup>2</sup> Institute for Astrophysical Research, Boston University, 725 Commonwealth Avenue, Boston, MA 02215, USA

<sup>3</sup> Institut de Radio Astronomie Millimétrique, 300 Rue de la Piscine, 38406 St. Martin d'Hères, France

<sup>4</sup> Max-Planck-Institut für Radioastronomie, Auf dem Hügel, 69, D-53121, Bonn, Germany

<sup>5</sup> Instituto de Radio Astronomía Milimétrica, Avenida Divina Pastora, 7, Local 20, E-18012 Granada, Spain

<sup>6</sup> School of Physics and Astronomy, University of Southampton, Southampton SO17 1BJ, UK

Preprint online version: October 15, 2018

## ABSTRACT

*Context.* A number of millimeter and submillimeter facilities with linear polarization observing capabilities have started operating during last years. These facilities, as well as other previous millimeter telescopes and interferometers, require bright and stable linear polarization calibrators to calibrate new instruments and to monitor their instrumental polarization. The current limited number of adequate calibrators implies difficulties in the acquisition of these calibration observations.

*Aims.* Looking for additional linear polarization calibrators in the millimeter spectral range, in mid-2006 we started monitoring 3C 286, a standard and highly stable polarization calibrator for radio observations.

*Methods.* Here we present the 3 and 1 mm monitoring observations obtained between September 2006 and January 2012 with the XPOL polarimeter on the IRAM 30 m Millimeter Telescope.

*Results.* Our observations show that 3C 286 is a bright source of constant total flux with 3 mm flux density  $S_{3\text{mm}} = (0.91 \pm 0.02)$  Jy. The 3 mm linear polarization degree ( $p_{3\text{mm}} = [13.5 \pm 0.3]\%$ ) and polarization angle ( $\chi_{3\text{mm}} = [37.3 \pm 0.8]^\circ$ , expressed in the equatorial coordinate system) are also constant during the time span of our observations. Although with poorer time sampling and signal-to-noise ratio, our 1 mm observations of 3C 286 are also reproduced by a constant source of 1 mm flux density ( $S_{1\text{mm}} = [0.30 \pm 0.03]$  Jy), polarization fraction ( $p_{1\text{mm}} = [14.4 \pm 1.8]\%$ ), and polarization angle ( $\chi_{1\text{mm}} = [33.1 \pm 5.7]^\circ$ ).

*Conclusions.* This, together with the previously known compact structure of 3C 286 –extended by  $\sim 3.5''$  in the sky– allow us to propose 3C 286 as a new calibrator for both single dish and interferometric polarization observations at 3 mm, and possibly at shorter wavelengths.

**Key words.** Polarization – Instrumentation: polarimeters – Techniques: polarimetric – Galaxies: quasars: individual: 3C 286 – Submillimeter: general – Radio continuum: general

## 1. Introduction

Despite the recent start of operations of a considerable number of millimeter observing facilities with ability for high precision polarization measurements (e.g., ALMA, PLANK, IRAM 30m Telescope and PdB Interferometer, SMA, KVN, BOOMERANG, CBI, MAXIPOL, QUaD, WMAP, and BICEP), the number of suitable polarization calibrators is still limited. The most commonly used sources for calibration of millimeter polarization observations are the Crab nebula (Taurus A, Aumont et al. 2010), Centaurus A (Zemcov et al. 2010), the limb of the Moon (Barvainis et al. 1988; Thum et al. 2003), and the diffuse Galactic emission (Matsumura et al. 2010). An ideal linearly polarized calibrator is a point-like, bright and constant source of high linear-polarization fraction with well defined and constant polarization angle. For most facilities designed to study the polarization properties of the cosmic microwave background, which still do not aim at observations with angular resolutions much better than  $\sim 5'$ , one or more among the four calibrators mentioned above fulfill most of these conditions. However, the relatively large angular extension of all these four polarization

calibrators ( $\geq 5'$ , where  $5'$  is the approximate angular extension of the Crab nebula at millimeter wavelengths; Aumont et al. 2010) may make difficult polarization calibration observations at angular resolutions better than that. Even when this is not the case, the poor coverage of adequate calibrators in the sky often reveals the need for new polarized sources suitable for calibration.

In this paper we present the results from series of millimeter measurements with the IRAM 30m Telescope to characterize 3C 286 (with J2000 equatorial coordinates:  $\alpha = 13^{\text{h}} 31^{\text{m}} 8.3^{\text{s}}$ ,  $\delta = +30^\circ 30' 33''$ ) as a new bright, compact, stable, and highly polarized calibrator for short millimeter observations. This source has been widely used for calibration at centimeter radio wavelengths both for total flux (Baars et al. 1977; Ott et al. 1994; Kraus et al. 1999) and linear polarization observations (Perley 1982; McKinnon 1992; Taylor et al. 2001; Gómez et al. 2002).

3C 286 is a bright compact steep spectrum radio quasar (Peacock & Wall 1982; Fanti et al. 1985) at a redshift  $z = 0.849$  (Burbidge & Burbidge 1969). Radio imaging with the Very Large Array at sub-arcsecond resolution has revealed an

extended structure composed of three misaligned bright features (e.g., Akujor & Garrington 1995). Among these three structures, the second one in brightness is located 2.6'' West–South–West from the brightest one. Both of them are linked by a nearly straight jet-like bridge of radio emission seen in high dynamic range images. The third emission region is located at 0.8'' East from the brightest one. Among these three emission features, the two brightest ones dominate the linear polarization emission, and show their electric vector oriented nearly parallel to the axis of the jet like structure between them. The integrated electric vector polarization angle of the source<sup>1</sup>  $\chi \approx 33^\circ$  at all observing wavelengths from 20 cm to 7 mm (Perley 1982; Taylor et al. 2001), see also <http://www.vla.nrao.edu/astro/calib/polar/>. The stability of  $\chi$  along radio frequencies has also been demonstrated through polarization angle rotation measure studies (Rudnick & Jones 1983). Very long baseline interferometric radio observations at milliarcsecond resolution of the brighter, and more compact, feature have revealed a well defined jet structure initially oriented in the South–West direction up to scales  $> 60$  milliarcseconds, with the linear polarization fraction ranging from  $p \approx 1\%$  and  $p \approx 20\%$  and  $\chi$  oriented nearly (but not exactly) parallel to the local jet axis (Jiang et al. 1996). These properties are not uncommon in radio loud quasar jets. However, 3C 286 lacks a highly variable, low polarization, and high brightness temperature ( $T_b \gtrsim 10^{10}$ – $10^{11}$  K) radio core (Cotton et al. 1997), as typical for radio quasars. This makes 3C 286 an excellent total flux and polarization calibrator at radio wavelengths, and provides it with its characteristic non variable, and large integrated linear polarization degree ( $p \approx 11\%$ ) at radio frequencies (<http://www.vla.nrao.edu/astro/calib/polar/>). The lack of a typical radio core in 3C 286 was interpreted by Cotton et al. (1997) as produced by strong relativistic de-boosting of the emission from the core when beamed in a direction significantly different from that of the observer’s line of sight.

## 2. Observations and data reduction

The observations presented here were performed with the XPOL polarimeter (Thum et al. 2008) on the IRAM 30 m Telescope. The 3C 286 measurements were taken for calibration purposes under the POLAMI (Polarimetric AGN Monitoring at the IRAM-30 m-Telescope) and the MAPI (Monitoring of AGN with Polarimetry at the IRAM-30 m-Telescope) programs (e.g., Agudo et al. 2011b), and for a densely time sampled 3 mm polarimetric monitoring program of blazar OJ287 (Agudo et al. 2011a). The time range of 3C 286 observations covers from 24 of September, 2006 (RJD = 54003)<sup>2</sup> to 30 of January, 2012 (RJD = 55957); see Figs. 1 and 2, and Tables 1 and 2.

The standard XPOL set-up and calibration scheme introduced in Thum et al. (2008) and Agudo et al. (2010) were used. Those measurements performed before Spring 2009 made use of the orthogonal linearly polarized A100 and B100 heterodyne receivers tuned at 3 mm (86 GHz). After Spring 2009, we employed the new E090 and E230 pairs of orthogonal linearly polarized receivers at the IRAM 30 m Telescope to observe simultaneously at 3 mm and 1 mm (229 GHz), where the angular res-

**Table 1.** 3 mm photo-polarimetric data from 3C 286.

Date	RJD days	$S_{3\text{mm}}$ Jy	$P_{3\text{mm}}$ %	$\chi_{3\text{mm}}$ °
2006-09-24	54003	0.92 ± 0.05	15.6 ± 0.5	39.0 ± 1.0
2006-10-03	54012	1.03 ± 0.05	13.4 ± 0.4	40.0 ± 1.1
2006-10-13	54022	0.90 ± 0.05	12.2 ± 0.4	39.0 ± 1.6
2006-10-14	54023	0.94 ± 0.05	14.4 ± 2.1	40.0 ± 2.6
2006-11-16	54056	0.87 ± 0.04	12.8 ± 1.1	32.1 ± 1.9
2006-11-17	54057	0.85 ± 0.04	16.6 ± 0.6	39.5 ± 0.9
2006-11-22	54062	0.90 ± 0.04	13.9 ± 0.5	41.8 ± 2.2
2006-12-01	54071	0.92 ± 0.05	14.1 ± 0.8	37.1 ± 1.1
2007-01-03	54104	0.96 ± 0.05	14.0 ± 1.4	38.4 ± 1.5
2007-01-17	54119	0.97 ± 0.05	14.9 ± 0.4	41.9 ± 1.0
2007-01-29	54130	0.94 ± 0.05	13.4 ± 0.4	36.1 ± 1.0
2007-06-11	54262	0.83 ± 0.04	14.8 ± 0.7	31.1 ± 1.3
2007-08-07	54320	1.00 ± 0.05	...	...
2007-10-09	54383	0.85 ± 0.04	15.6 ± 0.4	37.4 ± 1.0
2008-05-04	54591	0.87 ± 0.06	13.3 ± 0.8	30.1 ± 1.9
2008-05-13	54600	0.95 ± 0.05	...	...
2008-12-29	54830	1.02 ± 0.05	13.5 ± 0.4	39.1 ± 1.1
2009-06-18	55001	0.87 ± 0.04	13.0 ± 0.3	39.4 ± 0.8
2009-07-30	55043	0.90 ± 0.04	14.9 ± 1.1	38.9 ± 1.3
2009-08-18	55062	0.90 ± 0.04	13.9 ± 0.4	36.6 ± 2.1
2010-05-05	55322	0.98 ± 0.05	13.6 ± 0.4	37.5 ± 2.4
2010-06-06	55354	0.94 ± 0.05	12.6 ± 0.3	37.3 ± 1.1
2010-06-16	55364	0.83 ± 0.04	13.5 ± 0.3	37.5 ± 0.7
2010-08-15	55424	0.83 ± 0.04	15.4 ± 0.3	38.4 ± 0.7
2010-10-12	55482	0.93 ± 0.05	13.0 ± 0.3	33.8 ± 0.8
2011-01-31	55593	0.87 ± 0.04	13.4 ± 0.3	33.0 ± 0.7
2011-02-07	55600	0.95 ± 0.05	13.5 ± 0.3	35.2 ± 0.7
2011-03-25	55646	0.94 ± 0.05	13.5 ± 0.2	38.5 ± 0.7
2011-04-10	55662	0.92 ± 0.05	13.4 ± 0.3	37.6 ± 0.7
2011-04-25	55677	0.90 ± 0.04	12.1 ± 0.3	39.4 ± 0.9
2011-05-04	55686	0.96 ± 0.05	13.2 ± 0.3	35.7 ± 0.7
2011-05-22	55704	0.89 ± 0.04	14.2 ± 0.3	36.2 ± 0.7
2011-05-24	55706	0.98 ± 0.05	15.1 ± 0.3	41.1 ± 0.6
2011-06-15	55728	0.74 ± 0.04	13.1 ± 0.3	37.9 ± 0.8
2011-09-04	55809	0.82 ± 0.04	13.6 ± 0.3	35.9 ± 0.8
2011-09-11	55816	0.87 ± 0.04	12.6 ± 0.3	40.0 ± 0.8
2011-10-11	55846	0.95 ± 0.05	12.2 ± 0.3	38.0 ± 0.8
2011-10-16	55882	0.95 ± 0.05	13.8 ± 0.3	34.5 ± 0.7
2012-01-03	55930	0.97 ± 0.05	13.3 ± 0.3	37.4 ± 0.7
2012-01-30	55957	1.02 ± 0.05	13.2 ± 0.2	37.4 ± 0.7

**Table 2.** 1 mm photo-polarimetric data from 3C 286.

Date	RJD days	$S_{1\text{mm}}$ Jy	$P_{1\text{mm}}$ %	$\chi_{1\text{mm}}$ °
2010-05-05	55322	0.40 ± 0.02	14.3 ± 2.1	38.6 ± 3.9
2010-06-06	55354	0.33 ± 0.02	...	...
2010-10-12	55482	0.34 ± 0.03	...	...
2011-01-31	55593	0.31 ± 0.02	18.0 ± 2.4	22.3 ± 3.9
2011-02-07	55600	0.34 ± 0.02	13.9 ± 2.5	30.8 ± 5.0
2011-03-25	55646	0.28 ± 0.02	17.7 ± 3.4	35.8 ± 6.2
2011-04-10	55662	0.23 ± 0.01	17.5 ± 3.2	23.7 ± 5.2
2011-04-25	55677	0.21 ± 0.02	13.4 ± 5.5	19.3 ± 11.9
2011-05-04	55686	0.28 ± 0.02	18.5 ± 2.8	41.6 ± 4.0
2011-09-11	55816	0.26 ± 0.02	13.9 ± 4.7	38.1 ± 9.7
2011-10-11	55846	0.31 ± 0.02	17.0 ± 5.8	47.9 ± 8.6
2011-10-16	55882	0.34 ± 0.02	14.1 ± 2.5	32.2 ± 5.1
2012-01-03	55930	0.39 ± 0.02	10.2 ± 1.8	47.1 ± 5.4
2012-01-30	55957	0.36 ± 0.02	13.2 ± 2.1	23.8 ± 4.6

<sup>1</sup> To express polarization angles, we follow throughout this paper the IAU convention, which counts East from North in the equatorial coordinate system.

<sup>2</sup> RJD, i.e. reduced Julian date = Julian Date – 240000 days

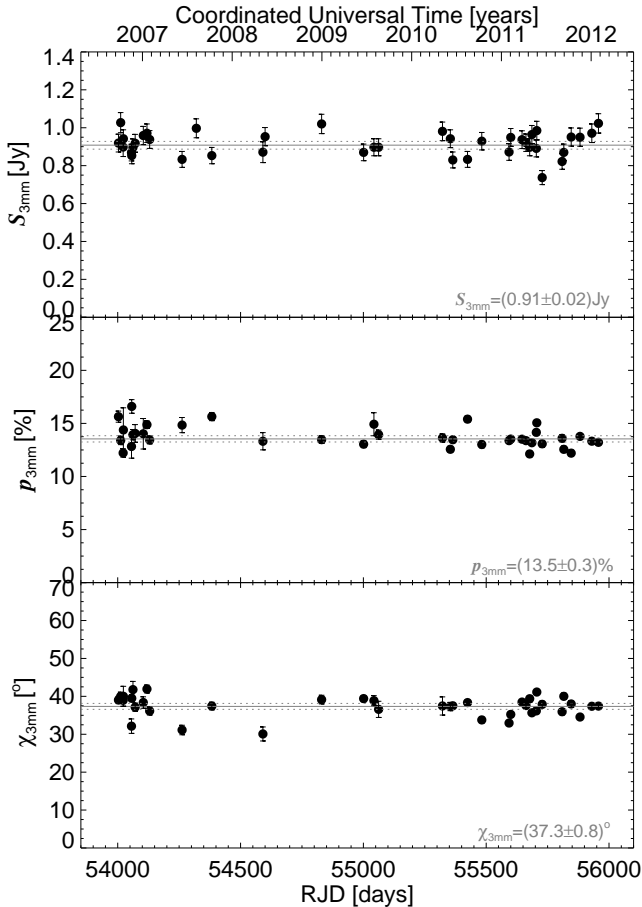


**Fig. 1.** 3 mm total flux and polarization evolution of 3C 286. The fitted constant values of  $S_{3\text{mm}}$ ,  $p_{3\text{mm}}$ , and  $\chi_{3\text{mm}}$  to be used for calibration through observations of 3C 286, and their 95 % confidence interval (obtained in Section 3.1), are given on every panel. The horizontal continuous and dotted lines symbolize such constant and 95 % interval, respectively.

olution of the telescope (full with at half power) is  $28''$  and  $11''$ , respectively.

After a cross-scan pointing of the telescope and an amplitude, and phase calibration measurement (see Thum et al. 2008), every XPOL measurement consisting of wobbler switching on-offs was performed for a total integration time  $\sim 8$  min. The signal from every one of the two orthogonal 3 mm receivers was connected to the XPOL polarimeter, whose output consisted of a 640 MHz spectrum from each one of such receivers, plus the real and imaginary part of their cross-correlation. These four XPOL observables are used to compute the 4 Stokes parameters for each measurement (Thum et al. 2008). XPOL hardware limitations only allow to connect 320 MHz to the remaining bandwidth of the polarimeter. This bandwidth was used for the simultaneous 1 mm observations taken after the end of 2009.

After calibration of the amplitudes and phases from every pair of linearly polarized orthogonal receiver, the instrumental polarization for every observing epoch (estimated through measurements of unpolarized calibrators, i.e. Mars and/or Uranus, when available) was removed from the data. The instrumental polarization parameters used for 3 mm observations before Spring 2009 were  $Q_i \approx 0.005I$ ,  $U_i \approx 0.003I$ , for the contribution of the instrumental polarization to the  $Q$  and  $U$  Stokes parameters, respectively. After mid 2009, new instrumental polarization parameters characterized the performance of the new

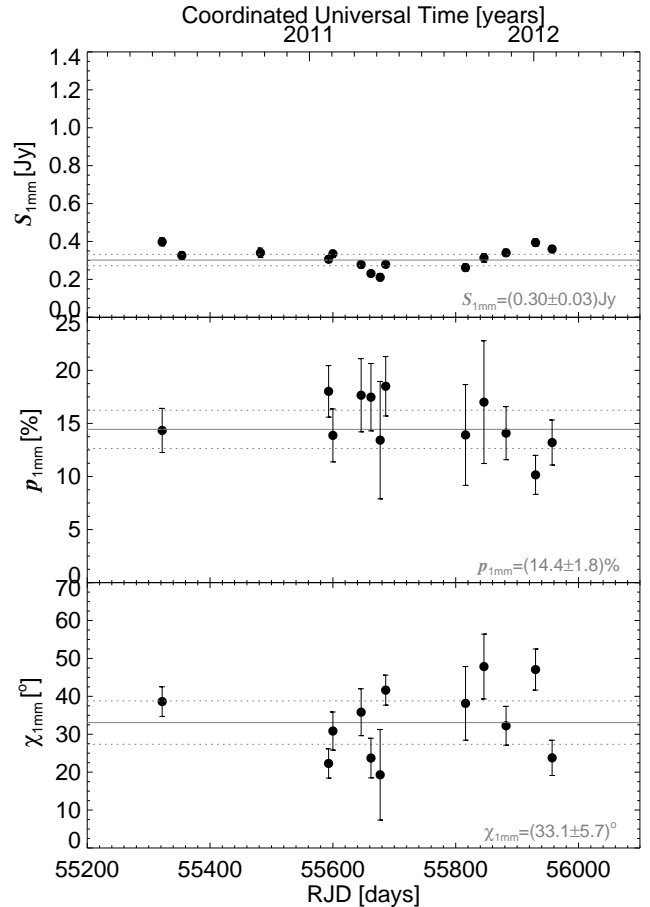


**Fig. 2.** Same as Fig. 1 but for the 1 mm data.

E090 and E230 receiver pairs on the 30 m Telescope. These are  $Q_i \approx -0.007I$  and  $U_i \approx -0.003I$  for 3 mm observations and  $Q_i \approx -0.015I$  and  $U_i \approx -0.015I$  for 1 mm. The Jy/K calibration factor ( $C_{\text{Jy/K}}$ ) for the total flux density scales were computed for every observing epoch before Spring 2009 as in Agudo et al. (2006). The resulting  $C_{\text{Jy/K}}$  values were fully consistent with the standard  $C_{\text{Jy/K}}$  calibration factors at 3 and 1 mm for the IRAM 30 m Telescope (6.4 Jy/K and 9.3 Jy/K, respectively; H. Ungerechts, private communication). For epochs after mid 2009 we used such standard  $C_{\text{Jy/K}}$  calibration factors.

The total flux density uncertainties given in Tables 1 and 2 correspond to the statistical uncertainties for every specific measurement plus a 5 % systematic factor from the uncertainties in  $C_{\text{Jy/K}}$  (Agudo et al. 2006) that was added quadratically. The linear polarization degree ( $p$ ) and linear polarization angle ( $\chi$ ) uncertainties in Tables 1 and 2 were estimated from the statistical uncertainties from every measurement, plus a non-systematic contribution computed from the dispersion of  $Q$ , and  $U$  Stokes parameters from measurements of Mars and Uranus. These dispersion estimates are  $\Delta Q_i = 0.003I$ , and  $\Delta U_i = 0.002I$ , for both 3 and 1 mm observations. These give polarization-uncertainty medians of  $\Delta p \approx 0.5\%$ ,  $\Delta \chi \approx 1^\circ$  at 3 mm, and  $\Delta p \approx 4\%$ ,  $\Delta \chi \approx 5^\circ$  at 1 mm for our measurements of 3C 286. The absolute calibration of the polarization angle of the XPOL polarimeter has a precision of  $0.5^\circ$  or better (Thum et al. 2008; Aumont et al. 2010). Hence, we do not consider a significant source of error from such calibration on the uncertainties of our final measurements.

### 3. Results and Discussion

#### 3.1. 3 mm

Figure 1 shows the 3 mm total flux density ( $S_{3\text{mm}}$ ), linear polarization degree ( $p_{3\text{mm}}$ ), and polarization angle ( $\chi_{3\text{mm}}$ ) evolution of 3C 286 as measured from mid 2006 to the beginning of 2012 (see also Table 1). Neither  $S_{3\text{mm}}$ , nor  $p_{3\text{mm}}$  and  $\chi_{3\text{mm}}$  show appreciable variability during the time range of our observations. Indeed, Fig. 1 resembles the behavior of a non varying total flux and polarization source, as observed for 3C 286 at longer centimeter wavelengths.

To verify the stability of  $S_{3\text{mm}}$ ,  $p_{3\text{mm}}$ , and  $\chi_{3\text{mm}}$  with time, we test if these variables can be fitted by a constant. Initially we fit a linear model to each one of these data sets. This model is characterized by a slope ( $b$ ) and an intercept ( $a$ ), i.e.  $y = a + bt$ , where  $t$  is the time and  $y$  is either  $S_{3\text{mm}}$ ,  $p_{3\text{mm}}$ , or  $\chi_{3\text{mm}}$ . The resulting linear-model best-fit parameters are given in Table 3. We tested the hypothesis that the slope  $b$  is equal to 0 (which we took as the Null Hypothesis,  $H_0$ ). In Table 3 we show that, for the case of  $b$ , the  $P$ -values coming from the  $t$ -statistic are 62%, 6% and 29% for  $S_{3\text{mm}}$ ,  $p_{3\text{mm}}$ , and  $\chi_{3\text{mm}}$  respectively. This points out that the probabilities of getting the fitted values of  $b$  by chance are not small. Based on the values of the  $t$ -statistic, we also estimate the 95% confidence intervals for the fitted values of  $b$  (see Table 3). The zero-value (i.e.  $b = 0$ ) lies within all such 95% confidence intervals. Since the  $P$ -values are greater than the 5% significance level the data do not provide grounds for rejecting the  $H_0$  at 5% significance level. Therefore, the measurements of  $S_{3\text{mm}}$ ,  $p_{3\text{mm}}$ , and  $\chi_{3\text{mm}}$  are each one of them distributed around a constant value, within a 95% confidence level.

Fitting a constant model (i.e.,  $y = a$ ) to the data further verifies the above picture (see also Fig 1). This is demonstrated by the remarkably low  $P$ -values for obtaining the fitted value by chance (see Table 4). The resulting fitted constant of  $S_{3\text{mm}}$ ,  $p_{3\text{mm}}$ , and  $\chi_{3\text{mm}}$  for 3C 286, and their 95% confidence intervals are  $S_{3\text{mm}} = (0.91 \pm 0.02)\text{Jy}$ ,  $p_{3\text{mm}} = (13.5 \pm 0.3)\%$ , and  $\chi_{3\text{mm}} = (37.3 \pm 0.8)^\circ$  (see Table 4 and Fig. 1). We propose these as the values of  $S_{3\text{mm}}$ ,  $p_{3\text{mm}}$ , and  $\chi_{3\text{mm}}$  to use for calibration through observations of 3C 286.

#### 3.2. 1 mm

At 1 mm (Fig. 2 and Table 2), the shorter observing bandwidth, the poorer atmospheric transmission and receiver sensitivity, and weakness of the source at this wavelength, together with the poorer time coverage at this spectral range in our monitoring of 3C 286 does not allow us to easily discern by visual inspection the stable  $S_{1\text{mm}}$ ,  $p_{1\text{mm}}$ , and  $\chi_{1\text{mm}}$  pattern seen at 3 mm. However, for the linear fit of  $S_{1\text{mm}}(t)$ ,  $p_{1\text{mm}}(t)$ , and  $\chi_{1\text{mm}}(t)$  (Table 5), the probabilities of getting the fitted values of  $b$  by chance are also rather high; 99, 12 and 94 %, respectively. The 95% confidence intervals for the fitted values of  $b$ , for the cases of  $S_{1\text{mm}}(t)$ ,  $p_{1\text{mm}}(t)$ , and  $\chi_{1\text{mm}}(t)$ , also include  $b = 0$ . The corresponding  $P$ -values are greater than the 5% significance level. Thus, we can also confirm that the measurements of  $S_{1\text{mm}}$ ,  $p_{1\text{mm}}$ , and  $\chi_{1\text{mm}}$  are distributed around a constant value, within a 95% confidence level. This is confirmed by the constant fits to the 1 mm data sets. Their expected values, and 95% confidence intervals, are  $S_{1\text{mm}} = (0.30 \pm 0.03)\%$ ,  $p_{1\text{mm}} = (14.4 \pm 1.8)\%$ , and  $\chi_{1\text{mm}} = (33.1 \pm 5.7)^\circ$  (Table 6 and Fig. 2).

#### 3.3. Total flux and polarization properties of 3C 286 along the radio and millimeter spectrum

Figure 3 and Table 7 show the total flux density and linear polarization properties of 3C 286 along the millimeter and radio-centimeter spectrum (from 1 mm to 21 cm). The corresponding data comes from either the results presented on this paper, or those from Peng et al. (2000) and Taylor et al. (2001), see Table 7.

The flux density plot shows a monotonically decreasing spectral trend as those expected for optically-thin synchrotron emission from relativistic jets (e.g., Marscher & Gear 1985). Despite some moderated spectral-index jumps seen for the measurements with larger errors (Fig. 4 and Table 8), the spectral index also shows an overall decreasing pattern along the broad radio-millimeter spectral-range considered here. No evident spectral break is observed from Fig. 3, hence suggesting that the synchrotron radiation observed from 3C 286 at 1 mm through 21 cm was produced by a single electron population.

The 3 and 1 mm polarization properties of 3C 286 shown by Fig. 3 seem to be rather similar to those at longer wavelengths within a  $\sim 2\%$  fractional polarization, and  $\sim 4^\circ$  polarization angle. However, the 3 and 1 mm polarization degree ( $p_{3\text{mm}} \approx 13.5\%$  and  $p_{1\text{mm}} \approx 14.5\%$ , respectively) seem to increase slightly for decreasing wavelengths with regard to the fractional polarization at wavelengths longer than 3 mm (that lies at the [11, 12] % level). The polarization angle that we measure at 3 mm ( $\chi_{3\text{mm}} \approx 37^\circ$ ) is also moderately different than the one measured at longer wavelengths ( $\sim 33^\circ$ , see Fig. 3 and Table 7). Our 1 mm polarization angle measurement ( $\chi_{1\text{mm}} = 33 \pm 6^\circ$ ) has sufficiently large uncertainty to avoid discerning if the shorter wavelength polarization angle matches the values of the 3 mm measurements or those at longer wavelengths. We hope to solve this ambiguity by better constraining the 1 mm polarization angle of 3C 286 through the continued monitoring of the source that we currently perform at the IRAM 30 m Telescope.

The slightly different fractional polarization and polarization angle at the shorter wavelengths in 3C 286 can be explained if the fraction of tangled magnetic field decreases towards inner regions upstream in the jet. Some fraction of such tangled magnetic field is needed to explain the decreased fractional polarization observed in the entire radio and millimeter spectrum with regard to the predicted value for optically-thin polarized synchrotron-radiation ( $\sim 70\%$ , Pacholczyk 1970), if Faraday depolarization is negligible (which is clearly the case of 3C 286, see Fig. 3). Also, the bulk jet emission should be radiated from jet regions at inner upstream locations for shorter wavelengths, as usually observed through very long baseline interferometry in relativistic jets in active galactic nuclei (e.g., Sokolovsky et al. 2011). Within this scenario, the radiation emitted at shorter wavelengths from inner jet region, would show higher fractional polarization than the longer wavelength emission. The different polarization angles for radiation emitted from inner jet regions may be explained by a slightly different jet direction with regard to the jet section where the longer wavelength emission is radiated (e.g., Abdo et al. 2010). This can be easily accommodated within Cotton et al.'s model for 3C 286 (see Fig. 6 in Cotton et al. 1997), which uses a bend in the inner jet regions to explain the apparent lack of a high brightness temperature core –beamed away from Earth in their model– as the cause for the unusual total flux and polarization properties of the source.

**Table 3.** Best-fit linear model parameters for  $S_{3\text{mm}}(t)$ ,  $p_{3\text{mm}}(t)$ , and  $\chi_{3\text{mm}}(t)$ .

Par. (1)	Est. (2)	$\epsilon$ (3)	$t$ -stat (4)	$P$ (5)	95% Conf. Int. (6) (7)	
$S_{3\text{mm}}$						
$a$	0.915	0.018	51	$1.1 \times 10^{-36}$	0.879	0.951
$b$	$-7 \times 10^{-6}$	$1.4 \times 10^{-5}$	-0.5	0.62	$-4 \times 10^{-5}$	$2.2 \times 10^{-5}$
$p_{3\text{mm}}$						
$a$	14.18	0.36	39	$4 \times 10^{-31}$	13.45	14.91
$b$	$-5 \times 10^{-4}$	$2.4 \times 10^{-4}$	-1.9	0.06	$-9 \times 10^{-4}$	$3 \times 10^{-5}$
$\chi_{3\text{mm}}$						
$a$	38.19	0.88	43	$1.1 \times 10^{-32}$	36.41	39.98
$b$	$-6 \times 10^{-4}$	$6 \times 10^{-4}$	-1.07	0.29	$-1.8 \times 10^{-3}$	$6 \times 10^{-4}$

Note: Columns are as follows: (1) fitted parameter, (2) estimate from the fit, (3) standard error, (4)  $t$ -statistic, (5) its corresponding  $P$ -value, and (6) and (7) lower and upper limits of the 95% confidence interval, respectively.

**Table 4.** Best-fit constant model parameters for  $S_{3\text{mm}}(t)$ ,  $p_{3\text{mm}}(t)$ , and  $\chi_{3\text{mm}}(t)$ .

$a$ (1)	$\epsilon$ (2)	$t$ -stat (3)	$P$ (4)	95% Conf. Int. (5) (6)	
$S_{3\text{mm}}$					
0.908	0.010	89	$1.2 \times 10^{-46}$	0.887	0.928
$p_{3\text{mm}}$					
13.54	0.15	93	$2.2 \times 10^{-45}$	13.25	13.84
$\chi_{3\text{mm}}$					
37.35	0.38	97	$3 \times 10^{-46}$	36.57	38.13

Note: Columns are as follows: (1) estimate of  $a$  from the fit, (2) standard error, (3)  $t$ -statistic, (4) its corresponding  $P$ -value, and (5) and (6) lower and upper limits of the 95% confidence interval, respectively.

**Table 5.** Same as Table 3 but for the 1 mm data.

Par. (1)	Est. (2)	$\epsilon$ (3)	$t$ -stat (4)	$P$ (5)	95% Conf. Int. (6) (7)	
$S_{1\text{mm}}$						
$a$	0.303	0.120	2.5	$2.4 \times 10^{-2}$	0.046	0.560
$b$	$-8 \times 10^{-7}$	$8 \times 10^{-5}$	-0.009	0.99	$-1.8 \times 10^{-4}$	$1.8 \times 10^{-4}$
$p_{1\text{mm}}$						
$a$	16.84	1.61	10	$1.1 \times 10^{-6}$	13.25	20.43
$b$	$-6 \times 10^{-3}$	$4 \times 10^{-3}$	-1.7	0.12	$-1.4 \times 10^{-2}$	$2.0 \times 10^{-3}$
$\chi_{1\text{mm}}$						
$a$	33.46	5.69	6	$1.6 \times 10^{-4}$	20.78	46.13
$b$	$-1 \times 10^{-3}$	0.014	-0.08	0.94	-0.03	0.03

**Table 6.** Same as Table 4 but for the 1 mm data.

$a$ (1)	$\epsilon$ (2)	$t$ -stat (3)	$P$ (4)	95% Conf. Int. (5) (6)	
$S_{1\text{mm}}$					
0.302	0.014	21	$1.2 \times 10^{-12}$	0.272	0.332
$p_{1\text{mm}}$					
14.44	0.82	18	$2.0 \times 10^{-9}$	12.64	16.24
$\chi_{1\text{mm}}$					
33.07	2.60	13	$6 \times 10^{-8}$	27.35	38.80

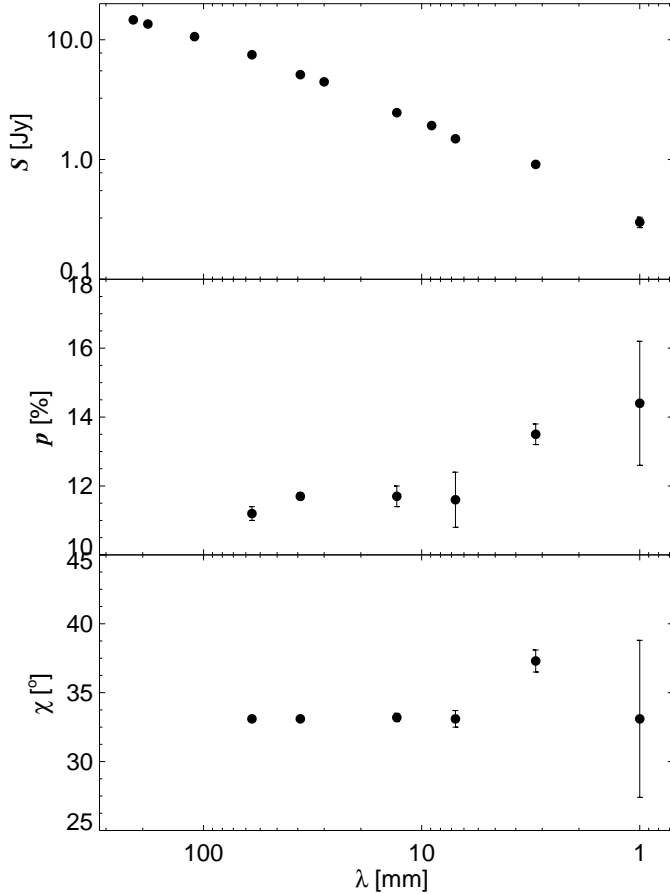


**Fig. 3.** Total flux density, polarization degree, and polarization angle of 3C 286 along the radio and millimeter spectrum. Plotted data are those presented in Table 7.

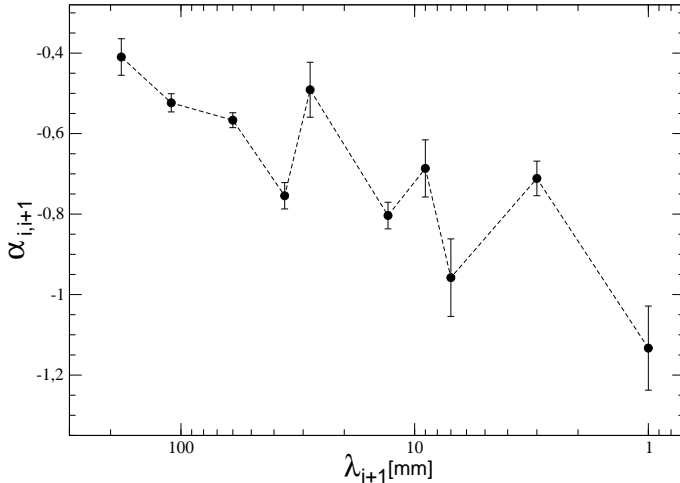


**Fig. 4.** Spectral index of 3C 286 as a function of  $\nu_{i+1}$ . The data presented here are those in Table 8.

#### 4. Summary and conclusions

We have shown that although 3C 286 displays moderate millimeter flux densities ( $S_{3\text{mm}} \approx 1$  Jy and  $S_{1\text{mm}} \approx 0.3$  Jy), its large millimeter polarization degree ( $p_{3\text{mm}} \approx 13.5\%$  and  $p_{1\text{mm}} \approx 14.5\%$ ) and its time stability make this source a valuable polarization calibrator for millimeter observations with instruments sensitive enough to detect linear polarization as bright as  $\sim 120$  mJy at 3 mm and  $\sim 45$  mJy at 1 mm.

**Table 7.**  $S$ ,  $p$ , and  $\chi$  measurements of 3C 286 along the millimeter and radio spectrum.

$\lambda$ mm	$S$ Jy	$p$ %	$\chi$ °	Ref.
1 <sup>a</sup>	$0.30 \pm 0.03$	$14.4 \pm 1.8$	$33.1 \pm 5.7$	1
3 <sup>a</sup>	$0.91 \pm 0.02$	$13.5 \pm 0.3$	$37.3 \pm 0.8$	1
7	$1.49 \pm 0.03^b$	$11.6 \pm 0.8^c$	$33.1 \pm 0.6^c$	2,3
9	$1.92 \pm 0.03^b$	...	...	2
13	$2.46 \pm 0.05^b$	$11.7 \pm 0.3^c$	$33.2 \pm 0.3^c$	2,3
28	$4.45 \pm 0.06^b$	...	...	2
36	$5.11 \pm 0.07^b$	$11.7 \pm 0.1^c$	$33.1 \pm 0.1^c$	2,3
60	$7.49 \pm 0.07^b$	$11.2 \pm 0.2^c$	$33.1 \pm 0.2^c$	2,3
110	$10.62 \pm 0.07^b$	...	...	2
180	$13.53 \pm 0.11^b$	...	...	2
210	$14.65 \pm 0.05^b$	...	...	2

**Notes.** <sup>(a)</sup>  $S$ ,  $p$ , and  $\chi$  correspond to fitted values as presented in this work. <sup>(b)</sup> Average values of  $S$  are those presented by Peng et al. (2000). <sup>(c)</sup> Average values of measurements made during 2009 by Taylor et al. (2001), see <http://www.vla.nrao.edu/astro/calib/polar/2009/>.

**References.** (1) This paper; (2) Peng et al. (2000); (3) Taylor et al. (2001)

**Table 8.** Spectral indexes of flux densities for contiguous wavelengths as shown in Table 7.

$\lambda_{i+1}$ mm	$\nu_{i+1}$ GHz	$\lambda_i$ mm	$\nu_i$ GHz	$\alpha_{i,i+1}$
1	229	3	86	$-1.13 \pm 0.11$
3	86	7	43	$-0.71 \pm 0.04$
7	43	9	33	$-0.96 \pm 0.10$
9	33	13	22	$-0.69 \pm 0.07$
13	22	28	11	$-0.80 \pm 0.03$
28	11	36	8.4	$-0.49 \pm 0.07$
36	8.4	60	5	$-0.75 \pm 0.03$
60	5	110	2.7	$-0.57 \pm 0.02$
110	2.7	180	1.7	$-0.52 \pm 0.02$
180	1.7	210	1.4	$-0.41 \pm 0.05$

**Notes.** The spectral index is defined such that  $\alpha_{i,i+1} = \frac{\log(S_i/S_{i+1})}{\log(\nu_i/\nu_{i+1})}$ .

The 3 and 1 mm total flux and polarization properties of 3C 286 have been shown to be rather similar to those previously known at longer wavelengths, which further supports the suitability of extending the use of 3C 286 as total flux and polarization calibrator from radio towards short millimeter wavelengths. The slightly larger 3 and 1 mm fractional polarization of the source with regard to those at longer wavelengths ( $p \in [11, 12]\%$  from 7 mm to 6 cm), can be explained if the degree of tangled magnetic field in the jet decreases towards inner upstream jet regions. To explain the deviation of  $\sim 4^\circ$  of the 3 mm (and perhaps 1 mm) polarization angle with regard to that at longer wavelengths, a small bend in the inner jet regions is also needed, but this is fully consistent with previous models for 3C 286. The time-dependent behavior of the source at 3 and 1 mm has been shown to be as stable as it is well known to be at shorter millimeter and radio wavelengths, which also supports the idea of the suitability of 3C 286 for total flux and polarization calibration purposes.

Having 3C 286 as an additional polarization calibrator may be an advantage for calibration and/or observing programs with limited observing time, if no other reliable polarization calibrator lies in the sky during their observing window. 3C 286 has a maximum extension of up to  $\sim 3.5''$  on the plane of the sky. In contrast, other available polarization calibrators show extended structures as large as  $\sim 5'$ , e.g. the case of the Crab nebula (Aumont et al. 2010), or even  $\sim 12'$  for Cygnus A (Zemcov et al. 2010). Hence, 3C 286 may facilitate polarization calibration observations with high resolution interferometers such as ALMA, Plateau de Bure, or the Sub-mm Array on extended configurations. Moreover, given the moderate northern declination of 3C 286 (see Section 1) it can be observed comfortably from all northern millimeter observatories, and (at elevations up to  $\approx 30^\circ$ ) even from most southern millimeter observatories, including ALMA.

We conclude that 3C 286 may be safely used for calibration of both single dish and interferometric polarization observations at 3 mm, and possibly at shorter wavelengths.

*Acknowledgements.* The authors thank the anonymous referee for constructive revision of this paper. The observations with the IRAM 30 m Telescope were made remotely from many different places. We thank the Observatory staff for their competent support. The IRAM 30m Telescope is supported by INSU/CNRS (France), MPG (Germany), and IGN (Spain). This research has made use of the VLA/VLBA Polarization Calibration Database that was maintained by the National Radio Astronomy Observatory (NRAO) of the USA, until the end of 2009. The NRAO is a facility of the USA's National Science Foundation operated under cooperative agreement by USA's Associated Universities, Inc. This research was partly funded by the "Consejería de Economía, Innovación y Ciencia" of the Regional Government of Andalucía through grant P09-FQM-4784, and by the "Ministerio de Economía y Competitividad" of Spain through grant AYA2010-14844. DE acknowledges the Science and Technology Facilities Council (STFC) of the United Kingdom for support under grant ST/G003084/1.

## References

- Abdo, A. A., Ackermann, M., Ajello, M., et al., 2010, *Nature*, 463, 919  
 Agudo I., Krichbaum T. P., Ungerechts H., et al., 2006, *A&A*, 456, 117  
 Agudo I., Thum C., Wiesemeyer H., Krichbaum T. P., 2010, *ApJS*, 189, 1  
 Agudo I., Jorstad S. G., Marscher A. P., et al., 2011a, *ApJL*, 726, L13  
 Agudo I., Marscher A. P., Jorstad S. G., et al., 2011b, *ApJL*, 735, L10  
 Akujor C. E., Garrington S. T., 1995, *A&AS*, 112, 235  
 Aumont J., Conversi L., Thum C., et al., 2010, *A&A*, 514, 70  
 Baars J. W. M., Genzel R., Pauliny-Toth I. I. K., Witzel A., 1977, *A&A*, 61, 99  
 Barvainis R., Clemens D. P., Leach R., 1988, *AJ*, 95, 510  
 Burbidge G. R., Burbidge E. M., 1969, *Nature*, 224, 21  
 Cotton W. D., Fanti C., Fanti R., et al., 1997, *A&A*, 325, 479  
 Fanti C., Fanti R., Parma P., Schilizzi R. T., van Breugel W. J. M., 1985, *A&A*, 143, 292  
 Gómez J. L., Marscher A. P., Alberdi A., Jorstad S. G., Agudo I., 2002, VLBA Scientific Memorandum, 30, 1 (<http://www.vlba.nrao.edu/memos/sci/sci30memo.ps>)  
 Jiang D. R., Dallacasa D., Schilizzi R. T., et al., 1996, *A&A*, 312, 380  
 Kraus A., Quirrenbach A., Lobanov A. P., et al., 1999, *A&A*, 344, 807  
 Marscher A. P. & Gear, W. K., 1985, *ApJ*, 298, 114  
 Matsumura T., Ade P., Barkats D., et al., 2010, *Proc. of SPIE*, 7741, 77412O  
 McKinnon M. M., 1992, *A&A*, 260, 533  
 Ott M., Witzel A., Quirrenbach A., et al., 1994, *A&A*, 284, 331  
 Pacholczyk, A. G. 1970, *Radio astrophysics. Nonthermal Processes in Galactic and Extragalactic Sources* (San Francisco: Freeman)  
 Peacock J. A., Wall J. V., 1982, *MNRAS*, 198, 843  
 Peng, B., Kraus, A., Krichbaum, T. P., Witzel, A., 2000, *A&AS*, 145, 1  
 Perley R. A., 1982, *AJ*, 87, 859  
 Rudnick L., Jones T. W., 1983, *AJ*, 88, 518  
 Sokolovsky, K. V., Kovalev, Y. Y., Pushkarev, A. B., Lobanov, A. P., 2011, *A&A*, 532, A38  
 Taylor, GB, Myers, ST, 2001, VLBA Scientific Memorandum, 26, 1 (<http://www.vlba.nrao.edu/memos/sci/sci26memo.ps>)  
 Thum C., Wiesemeyer H., Morris D., Navarro S., Torres M., 2003, *Proc. of SPIE*, 4843, 272  
 Thum C., Wiesemeyer H., Paubert G., Navarro S., Morris D., 2008, *PASP*, 120, 777

Zemcov M., Ade P., Bock J., et al., 2010, *ApJ*, 710, 1541